

# STSM Report

## Experimental characterization and parameterization of the load-to-grain angle dependent embedment behavior of dowel-type fasteners in laminated veneer lumber (LVL)

Michael Schweigler

Vienna University of Technology  
Institute for Mechanics of Materials and Structures  
Vienna, Austria

### 1 Introduction and objective of the STSM

Profound knowledge on the embedment behavior of steel dowels in wood and engineered wood based products is essential for a reliable design of dowel connections. Due to the inherent anisotropic mechanical nature of wood and wood products, a complex stress state in the wood below the interface with the steel dowel is evoked. As a further consequence of the anisotropy, significant differences in the embedment behavior between loading at different angles with respect to the grain direction are observed. Recent developments related to reinforcement techniques, allow for a pronounced ductile behavior of dowel connections, and thus, require information on the embedment behavior for dowel displacements beyond the displacement limits of current test and design standards.

Up to now only a few studies covered the experimental characterization of the embedment behavior beyond the 5 mm displacement limit of EN 383 (2007). Sandhaas et al. (2013) studied the embedment behavior parallel to the grain for various softwood and hardwood species up to a maximum dowel displacement of 15 mm. Bleron and Duchanois (2006) and Sawata and Yasumura (2002) carried out embedment tests on softwood species up to dowel displacements of 12 and 20 mm, respectively. Limited research was conducted on the embedment behavior at different load-to-grain angles. Ehlbeck and Werner (1992) investigated three load-to-grain angles between parallel and perpendicular to the grain using hardwood species and applied the so-called *Hankinson formula*, Hankinson (1921), as an interaction criterion. Further experimental investigations on the load-to-grain angle dependence were carried out for softwood by Bleron and Duchanois (2006), for European hardwood by Hübner et al. (2008) and for solid timber and LVL from radiata pine by Franke and Quenneville (2010). However, proposals for design equations have been limited to the assumptions of the European yield model, Johansen (1949), i.e., an assumed ideal plastic material behavior of wood, while pronounced hardening effects for load-to-grain angles close to 90° have been rarely considered for the engineering design of connections, e.g. Hochreiner et al. (2013).

Due to the anisotropic material behavior of wood, embedment stresses are additionally influenced by the lateral displacement boundary conditions of the steel dowel during loading. For load-to-grain angles in between the principal material directions of wood, a lateral displacement or a reaction force is encountered for unconstrained or constrained displacement boundary conditions, respectively, see

e.g. Bader et al. (2016). The corresponding effects could be related to the loading situation encountered for dowels in timber-to-timber and steel-to-timber connections, respectively. From a mechanical point of view, results from embedment tests with unconstrained lateral loading conditions can be interpreted as lower limit, and those from embedment tests with constrained lateral boundary conditions as upper limit of the corresponding embedment stresses.

The aim of the author's current project is to investigate the embedment behavior of laminated veneer lumber (LVL) under the above described loading conditions, i.e., loading at different load-to-grain angles up to dowel displacements beyond the displacement limits of current test standards, including unconstrained as well as constrained lateral displacement boundary conditions. The envisaged outcome of this project is a parameterized definition of the load-displacement behavior of dowel-type fasteners embedded in LVL, which is expected to support the standardization process and could be used as input to analytical and numerical models of dowel connections, facilitating an advanced description of the nonlinear behavior of dowel connections in timber structures.

Experimental investigations of the embedment behavior of LVL under constrained lateral displacement conditions, as well as discussion on possible parameterization strategies were the objective of the herein presented STSM project. The availability of a biaxial testing machine at the host institute, namely the *Linnæus University* in Växjö, Sweden, allowed for an execution of the experimental investigations. Thanks to this biaxial testing machine, it was possible to record, in addition to the vertically applied displacement loading, also the lateral reaction force, evoked by the anisotropic material behavior under constrained lateral displacement conditions. The herein gained data are expected to serve as a valuable input to design models and equations for steel-to-timber connections. Beside the load-displacement behavior, which constitutes an upper limit of the embedment stress, especially the transverse forces are important information for the modeling of the stress state in the surrounding wood matrix and thus for the design process in general.

Prior to the STSM, experimental characterization of the embedment behavior of LVL under unconstrained lateral displacement conditions was carried out at the author's home institute *Vienna University of Technology* (Vienna, Austria). Unconstrained loading conditions were enabled by load-application via a pendulum, see Schweigler et al. (2016). A non-contact displacement measurement system, based on digital image correlation (DIC) technique, was used in order to measure the in general nonlinear displacement path of the dowel, as a result of the anisotropic material behavior and unconstrained loading condition. Furthermore, DIC was used to record the strain distribution in the vicinity of the dowel, in order to support the interpretation of the displacement dependent bearing mechanisms and identification of local and global cracks. Promising results have been found from this test series, as regards the global load-displacement behavior and the local embedment behavior, see Schweigler et al. (2016).

For reasons of comparability, embedment test under constrained lateral displacement conditions in this STSM project were designed using the same materials and embedment testing conditions as applied for the already conducted embedment test series with unconstrained loading situation. In both test series, laminated veneer lumber (LVL) loaded by 12 mm and 16 mm dowels, under standard moisture conditions, at similar load-to-grain angles, up to similar dowel displacements, etc., were investigated. Therefore, a direct comparison of the data from both test series was possible. Furthermore, the data from both test series could be interpreted as a single dataset, representing an upper and lower limit of the embedment behavior in LVL, based on constrained and unconstrained loading situations, respectively. Evaluation of test data will include the calculation of embedment stresses as a function of the displacement and the load-to-grain angle, as well as embedment strength properties according to definitions in current testing and design standards. This will facilitate the comparison with previous data and include a proposal for design equations for future standard revisions. The output of these tests is also expected to support discussions related to testing regulations provided in testing standards.

The report is organized as follows: A description of the embedment test program under constrained and unconstrained lateral dowel displacement conditions, as well the applied methodology for

parameterization of the embedment behavior is given in Section 2. Selected results from these experiments are presented and discussed in Section 3, before conclusions are drawn and future collaborations with the host institution and planned publications are given in Section 4 and 5, respectively.

## 2 Materials and methods

### 2.1 Embedment tests under constrained lateral displacement boundary conditions

The experimental characterization of the embedment behavior of steel dowels embedded in LVL under constrained lateral displacement boundary conditions constituted the main part of the herein presented STSM. In total, more than 50 embedment tests under constrained displacement boundary conditions, including two different dowel diameters, namely 12 mm and 16 mm, were performed. The load was applied under  $0^\circ$ ,  $15^\circ$ ,  $30^\circ$ ,  $45^\circ$ ,  $60^\circ$ ,  $75^\circ$  and  $90^\circ$  with respect to the grain direction.

Laminated Veneer Lumber (LVL) with parallel oriented veneers made of spruce (Kerto-S<sup>®</sup>, Metsä, Finland), with a thickness of 51 mm was chosen. Wooden test specimens had a width and height of  $200 \times 200 \text{ mm}^2$ , except for load-to-grain angles,  $\alpha$ , of  $75^\circ$  and  $90^\circ$ , where an increased specimen width of 400 mm was used. A reinforcement by means of self-tapping screws (SPAX T-STAR plus, SPAX International GmbH & Co.KG, Germany), with a diameter of 8 mm was inserted into predrilled holes at a distance of 60 mm above and below the dowel. A summary of the specimen geometry, the number of tests per load-to-grain angle and dowel diameter are given in Table 1.

*Table 1: Dimensions of tested LVL specimens (cf. Figure 1).*

Load-to-grain angle ( $^\circ$ )	Width (mm)	Height (mm)	Thickness (mm)	Number of tests (-) for $d=12 \text{ mm}$	Number of tests (-) for $d=16 \text{ mm}$
0	200	200	51	3	3
15	200	200	51	4	4
30	200	200	51	4	4
45	200	200	51	5	4
60	200	200	51	4	4
75	400	200	51	4	4
90	400	200	51	3	3

Prior to testing, LVL samples were stored under standard climatic conditions of  $20^\circ \text{C}$  and 65% relative humidity, until mass equilibrium was reached. The mean mass density of the LVL samples amounted to  $510.5 \text{ kg/m}^3$  (stdv= $6.3 \text{ kg/m}^3$ ,  $n=53$ ). Small, kiln-dried LVL samples were used to determine the corresponding moisture content, which was found to be 11.0% (stdv= $0.08\%$ ,  $n=4$ ).

Dowels of high steel quality (hardened steel) with smoothed surface were used for both dowel diameters, in order to ensure only elastic bending deformations of the dowel, and thus quasi-uniform loading over the thickness of the specimen. In order to describe the surface quality of the steel dowels, the surface texture was recorded by means of a contact-free characterization technique. The arithmetic average of the surface roughness,  $R_a$ , amounted to  $1.14 \mu\text{m}$  (stdv= $0.029 \mu\text{m}$ ) and  $0.68 \mu\text{m}$  (stdv= $0.007 \mu\text{m}$ ) for the dowels with 12 mm and 16 mm in diameter, respectively. For galvanized steel dowels, Sandhaas et al. (2013) determined  $R_a$  values of  $0.88 \mu\text{m}$ . The steel dowels were inserted into predrilled holes without any clearance.

Embedment test were carried out as full-hole embedment tests under compression following the principles of EN 383 (2007). A biaxial test setup allowed for recording, in addition to the vertical loading, also the lateral reaction force, evoked by the anisotropic material behavior under constrained loading conditions (see Figure 1). The testing machine (MTS Model 661.20F) consisted of a vertical

and horizontal loading sledge, controlled independently from each other. The steel dowel, located in the center of the LVL specimen, was loaded in vertical direction by steel plates on both sides of the specimen. These steel plates were fixed to the vertical sledge of the testing machine (see Figure 1). To achieve testing under different load-to-grain angles, the specimens were cut under a corresponding angle out of the LVL boards. For loading under directions different from the principal material directions, vertical loading evoked a horizontal reaction of the specimen. This was a horizontal reaction force, since the specimen was fixed to the horizontal sledge with a steel support device, and the displacement of the horizontal sledge was held fixed, i.e. the displacement was set to zero during vertical load application (see Figure 1).

Loading was applied displacement controlled up to a displacement of at least two times the dowel diameter, i.e., 24 mm and 32 mm, for the 12 mm and 16 mm dowel, respectively. In addition, two unloading sequences, one in the quasi-elastic part, and one in the elasto-plastic part were performed. The first unloading sequence, was introduced at an embedment stress of approximately half the quasi-elastic stress limit. The second one was performed at a dowel displacement of about one times the dowel diameter. At the beginning of both unloading cycles, the force was kept constant for 5 sec, in order to reduce the influence of time dependent effects on the elastic unloading behavior. A constant displacement rate of 2 mm/min was used for all loading and unloading sequences.

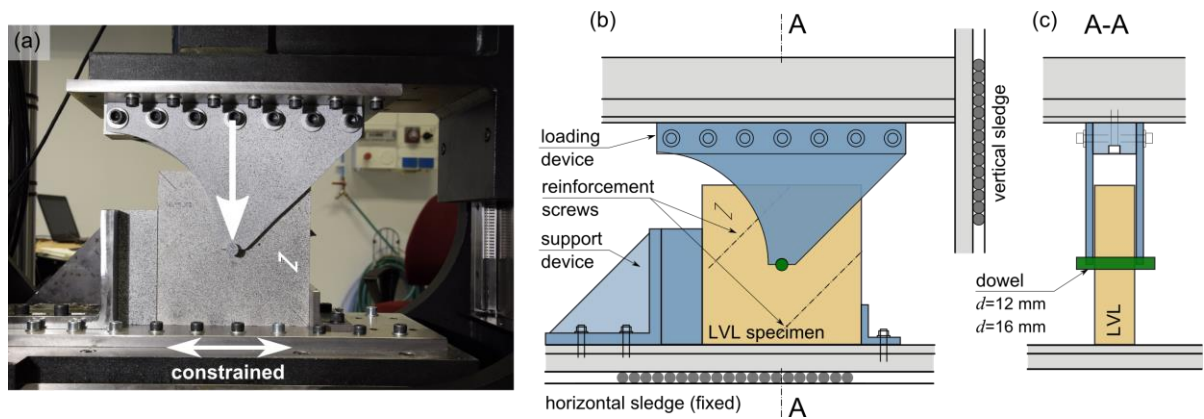


**Figure 1:** Test setup for full-hole embedment tests under constrained lateral displacement boundary conditions, (a) vertical loading; horizontal displacement constrained; for a load-to-grain angle of 45°, (b) sketch of the test setup for loading under 45° and (c) cross section through the test setup.

The load cells of the biaxial testing machine directly recorded vertical loading and horizontal reaction forces as a result of the prescribed vertical displacement. In contrast, the deformation behavior was measured separately by a non-contact displacement measurement system, based on digital image correlation (DIC) technique (Aramis®, GOM, Braunschweig, Germany). Combination of two 12 mpx cameras allowed for recording a three-dimensional displacement field of the specimen surface, the dowel head, the loading and the support device. Thus, the DIC system gave access to the dowel displacement relative to the LVL surface. In addition, DIC measurements allowed recording the strain field on the surface of the wooden specimen, which supports identification of bearing mechanism and cracks, as well as visualization of load distributions. The field of view was chosen to approximately 30x25 cm<sup>2</sup>. A facet size of 19 px and grid spacing of 15 px resulted in a distance of approximately 1.2 mm between the measurement points. In addition, selected specimens were cut along the middle plane of the LVL sample after testing for visual inspection. Thus, plastic deformations and failure mechanisms could be visualized, unaffected by unpreventable disturbing surface effects at large dowel displacements, like for example splitting of the outer veneers.

Vertical and lateral reaction forces, as a consequence of the applied vertical dowel displacement, were expressed as embedment stresses ( $f_{h,ver}$  and  $f_{h,lat}$ ). For this purpose, reaction forces were divided by the projected area of the dowel, i.e., by the thickness of the LVL specimen times the dowel diameter. Thus, embedment stresses are defined as nominal embedment stresses, assuming a uniform

embedment stress distribution over the dowel diameter (see also definitions specified in EN 383 (2007)).

Further parameters were calculated based on the embedment stress-displacement relationships, including strength parameters as embedment stresses at specific dowel displacements and stiffness properties during the loading and unloading sequences (see Schweigler et al., 2016 for more details on the parameters).

## 2.2 Embedment tests under unconstrained lateral displacement boundary conditions

The experimental characterization of the embedment behavior under unconstrained lateral displacement boundary conditions is another essential part of the author's current project, i.e., to investigate the embedment behavior of LVL at different load-to-grain angles up to large plastic dowel displacements. This experimental program was conducted prior to the STSM at the author's home institute (*Vienna University of Technology*, Vienna, Austria). Thus, this subsection gives only a brief overview of these tests, which are subsequently used in this project for comparison with the results from embedment tests under constrained lateral displacement boundary conditions (see Subsection 2.1). For detailed information related to this test series, the reader is referred to Schweigler et al. (2016).

In total, 85 full-hole embedment tests under unconstrained lateral displacement boundary conditions following the principles of EN 383 (2007) were carried out. Similar testing conditions as described in Subsection 2.1 were used i.e., the same materials, climatic conditions, specimen geometry, loading procedure, as for the embedment tests under constrained displacement boundary conditions. Experiments were conducted for two different dowel diameters, namely 12 mm and 16 mm, loaded under 0°, 15°, 30°, 45°, 60°, 75° and 90° to the grain.

Again, LVL with parallel oriented veneers of spruce (Kerto-S®) was used. Specimen thickness was 51 mm, width and height were 200 mm, except for loading perpendicular to the grain (90°) the specimen width was increased to 400 mm. A reinforcement by means of self-tapping screws (SPAX T-STAR plus), with 8 mm in diameter was inserted above and below the dowel. Tests were carried on specimens equilibrated at standard climatic conditions of 20° and 65% relative humidity. Similar mass densities and moisture contents as for the test series with constrained dowel displacement boundary conditions were found. The same steel dowels produced from hardened steel with smoothed surface were used.

As regards the test setup, a special support device was used for testing at various load-to-grain angles. It consisted of a rectangular V-shaped steel structure, which rested on a circular construction (Figure 2). The latter could be rotated relative to each other allowing testing between 0° and 90° with respect to the grain direction. This support device allowed to cut the specimens in a rectangular shape parallel and perpendicular to the grain direction of the LVL boards, which differs from cutting the specimens at the corresponding load-to-grain angle, as it was used for the test series at constrained loading conditions (see Subsection 2.1). Steel elements on both sides of the specimen constituted the loading device, which acted as a pendulum with the center of rotation at the contact point fixed to the cross head of the testing machine (see Figure 2). Due to the pendulum, the dowel displacement was not constrained perpendicular to the loading direction, and thus able to follow the in general nonlinear displacement path.

A digital image correlation measurement system (Q-400, Dantec Dynamics, Germany) with two pairs of 5 mpx cameras, one on each side of the test setup, was applied. Thus, the in general nonlinear displacement path of the dowel, and the strains on the surface of the LVL specimen could be recorded. The vertical reaction force was directly recorded by the load cell of the testing machine.

Embedment stress-displacement relationships and characteristic parameters were calculated as outlined in Subsection 2.1.

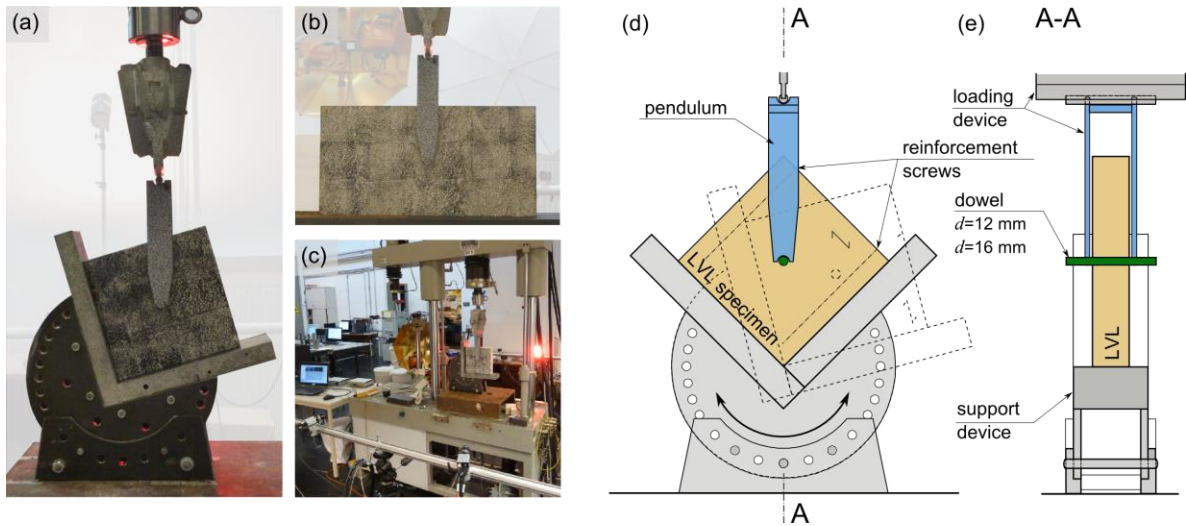


**Figure 2:** Test setup for full-hole embedment tests under unconstrained lateral displacement boundary conditions, (a) test setup for  $\alpha=15^\circ$ , (b)  $\alpha=90^\circ$ , (c) DIC-measurement system, (d) sketch of the test setup for loading under  $45^\circ$  to the grain and (e) cross section through the test setup; see also Schweigler et al. (2016).

### 2.3 Parameterization of the embedment behavior

Based on the experimental results obtained from the test series presented in Subsections 2.1 and 2.2, different methods to parameterize the embedment stress-displacement behavior regarding its dependence on the load-to-grain angle,  $\alpha$ , were discussed. Such a parameterized definition of the embedment behavior would have the advantage of a direct accessibility of the embedment stress for arbitrary load-to-grain angles and dowel displacements, as it is the case for single dowels, being part of a dowel group, see e.g. Bader et al (2015a) and Bader et al (2015b). Thus, the parameterized definition of the embedment stress could be used as input to analytical and numerical models of the nonlinear behavior of dowel connections. The intention of the discussions performed during this STSM was to find regression functions, already used in timber engineering applications, based on the goal of as less input parameters as possible to describe the embedment behavior. The following presented two step approach has been found to be most suitable for this purpose:

In a first step, the following exponential regression function, for example presented by Foschi (1974), was used to fit the single experimentally determined slip curves for each load-to-grain angle separately (see Figure 3a), reading as

$$f_{h,i}(u_i, \alpha_i) = (f_{h,in,\alpha} + k_{f,\alpha} \cdot u_i) \cdot \left[ 1 - e^{-\frac{k_{0,\alpha} \cdot u_i}{f_{h,in,\alpha}}} \right]. \quad (1)$$

Eq. (1) gives the embedment stress  $f_{h,i}$  as function of the dowel displacement  $u_i$  for a specific load-to-grain angle  $\alpha$ . The coefficient  $k_{0,\alpha}$  describes the initial embedment stiffness,  $k_{f,\alpha}$  specifies the tangent stiffness of the elasto-plastic loading path and  $f_{h,in,\alpha}$  is related to the embedment stress at the intersection of the two stiffness paths. The least square method is used to determine these three coefficients. Applying Eq. (1) to each experimentally determined slip curve for the different load-to-grain angles,  $\alpha$ , results in three coefficients for each  $\alpha$ .

In a second step, the so-called *Hankinson's formula*, Hankinson (1921), was applied to each of these three coefficients to give a regression between these coefficients and the load-to-grain angle  $\alpha$  (see Figure 3b-d). These three regression functions read as

$$f_{h,in,\alpha} = \frac{f_{h,in,0} \cdot f_{h,in,90}}{f_{h,in,0} \sin^m \alpha + f_{h,in,90} \cos^m \alpha}, \quad (2)$$

$$k_{f,\alpha} = \frac{k_{f,0} \cdot k_{f,90}}{k_{f,0} \sin^m \alpha + k_{f,90} \cos^m \alpha}, \quad (3)$$

$$k_{0,\alpha} = \frac{k_{0,0} \cdot k_{0,90}}{k_{0,0} \sin^m \alpha + k_{0,90} \cos^m \alpha}. \quad (4)$$

Each regression function includes two coefficients, which are related to the embedment behavior at  $\alpha=0^\circ$  and  $\alpha=90^\circ$ . At the same time, the shape of the curve between the two limit values at  $0^\circ$  and  $90^\circ$  to the grain can be controlled by the exponent  $m$  of the trigonometric functions. Again the least square method was applied to determine the corresponding coefficients. Thus, the embedment stress,  $f_h$ , dependent on the dowel displacement,  $u$ , and load-to-grain angle,  $\alpha$ , can be described by in total six coefficients, by inserting Eqs. (2)-(4) into Eq. (1) (cf. Figure 3e). The exponent  $m$  was used to adjust the regression functions for the two different lateral displacement boundary conditions investigated in the above-described test series.

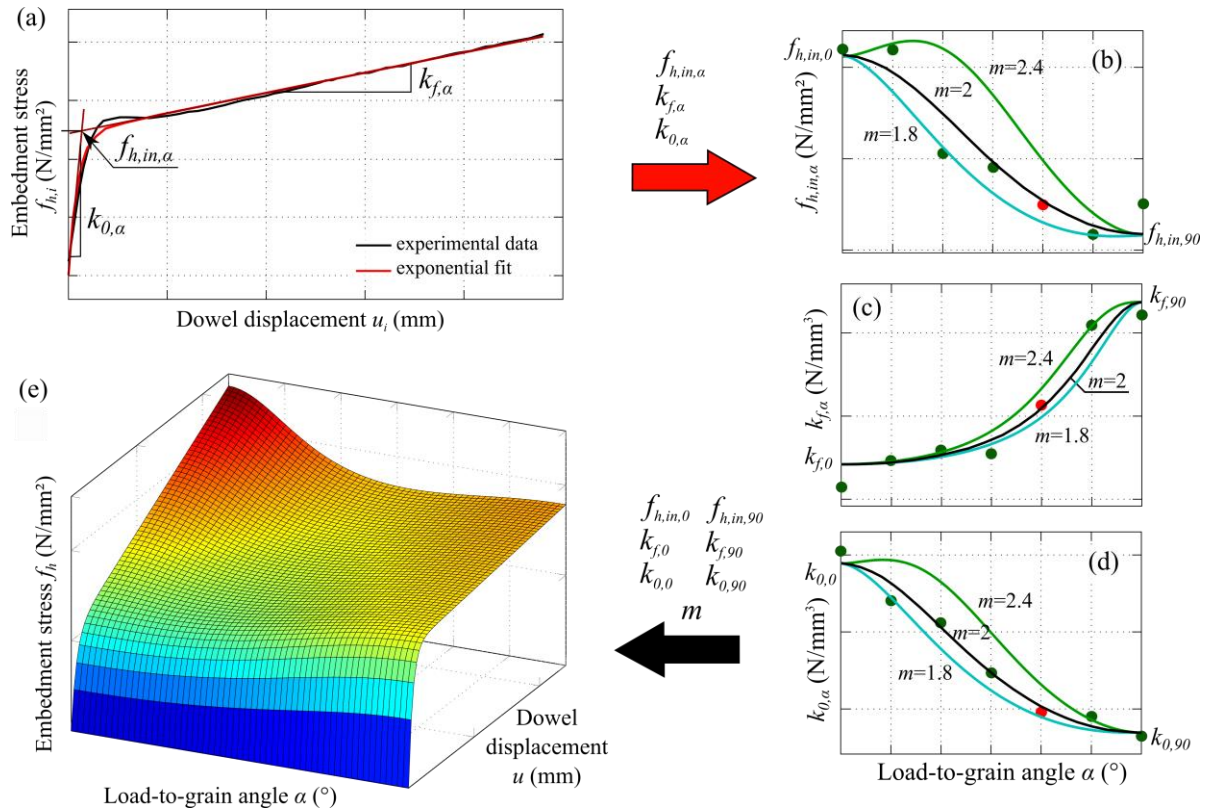


**Figure 3:** Procedure for parameterization of the embedment behavior, (a) fitting of the experimental slip curves per load-to-grain angle, (b)-(d) fitting of the coefficients gained from (a), (e) parameterized embedment behavior based on  $m=2$  as function of the load-to-grain angle,  $\alpha$ , and dowel displacement,  $u$ .

### 3 Results and discussion

Section 3 gives a brief overview of selected results gained from the experimental program related to the behavior of steel dowels embedded in laminated veneer lumber (LVL). Subsection 3.1 and Subsection 3.2 describe results of embedment tests under constrained and unconstrained lateral displacement boundary conditions, respectively. A comparison between these two test series is given in Subsection 3.3.

#### 3.1 Embedment tests under constrained lateral displacement boundary conditions

This subsection represents a selection of results from the embedment tests under constrained lateral displacement boundary conditions carried out during the STSM at the *Linnæus University* (Växjö, Sweden). In general, a pronounced ductile behavior was observed for all tested combinations of different dowel diameters and load-to-grain angles. Only for loading parallel and close to parallel to the grain, minor splitting on the specimen surface was seen, which however did not lead to premature failure of the specimens, since these were reinforced by self-tapping screws.

Distinct nonlinear relations between the embedment stress and dowel displacement, as well as the load-to-grain angle were observed. Figure 4a shows a three-dimensional illustration of the embedment stress plotted over the dowel displacement and load-to-grain angle, for dowels with a diameter of 12 mm. Linear interpolation has been used for the areas between the experimentally determined slip curves. In Figure 4b, the corresponding load-displacement curves are plotted separately for each load-to-grain angle. In general, a similar shape of the load-displacement curves has been found for both dowel diameters of 12 mm and 16 mm, however, differences in the magnitude of the nominal embedment stress, dependent on the load-to-grain angle and dowel displacement, between these two dowels were observed. In the following, results are presented exemplarily for the 12 mm dowel.

The load-displacement behavior of the vertical embedment stress can roughly be described by a quasi-linear elastic behavior, followed by a pronounced, almost linear plastic behavior consistently for all investigated load-to-grain angles. As regards the vertical embedment stress, caused by the prescribed vertical dowel displacement, three distinct areas of similar behavior can be defined. For loading parallel to the grain ( $0^\circ$ ) up to loading under  $30^\circ$  to the grain, the load-displacement behavior can be characterized by an almost linear-elastic, ideal plastic response (cf. Figure 4b). A decrease in the quasi-elastic stiffness and embedment strength with increasing load-to-grain angle,  $\alpha$ , can be seen. The area for loading between  $30^\circ$  and  $60^\circ$  with respect to the grain, exhibits a further decrease in the quasi-elastic strength limit, and additionally a pronounced increase of the elasto-plastic stiffness with increasing  $\alpha$ . For loading under  $60^\circ$  to the grain and higher, almost the same behavior regarding stiffness and strength for the quasi-elastic and elasto-plastic part was seen. The corresponding increase of the elasto-plastic loading stiffness with increasing  $\alpha$ , could be explained by densification of the wood in the contact area below the dowel as well as by a rope effect in the wood fibers. The latter effect is related to stresses parallel to the grain, which can arise for load components perpendicular to the grain, as a consequence of deflection forces gained from wood fibers in bending. In addition, the densification effect in the wood below the dowel is superimposed by strengthening effects caused by the constrained load application. This strengthening effect is expected to be strongest for load-to-grain angles with the highest lateral embedment stresses, which will be discussed next.

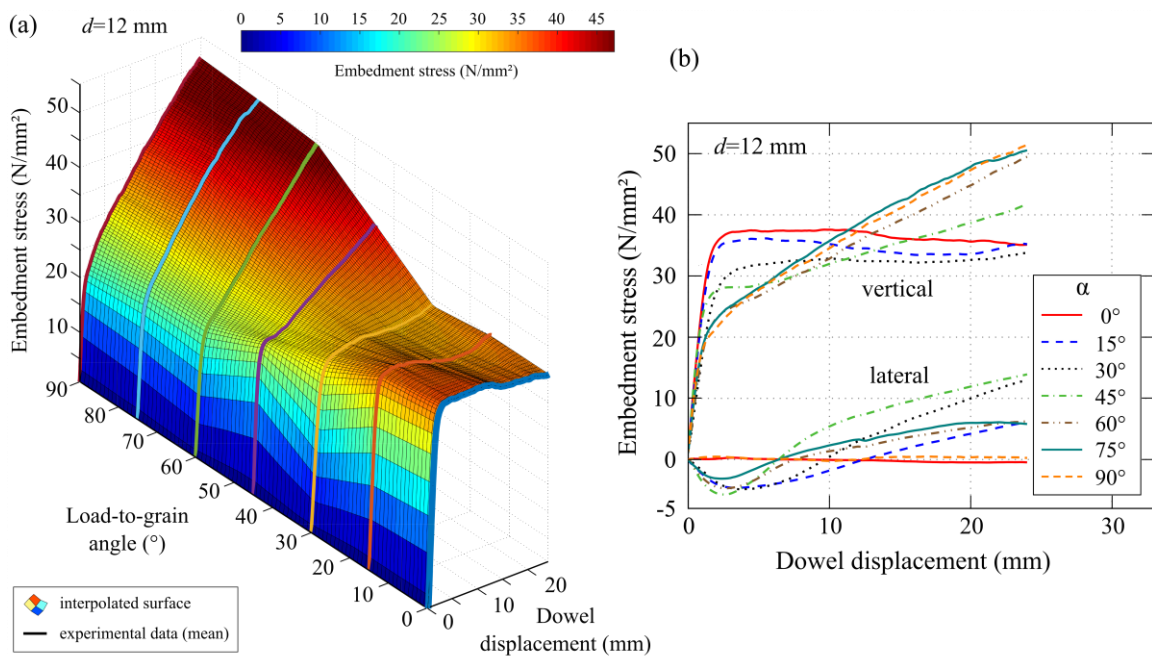


**Figure 4:** Embedment behavior under constrained lateral dowel displacement boundary conditions for  $d=12$  mm, (a) embedment stress plotted over the load-to-grain angle and the dowel displacement, (b) vertical and lateral embedment stresses plotted over the dowel displacement for different load-to-grain angles.

Constraining a vertical dowel displacement evokes in addition to the vertical reaction force also a lateral (horizontal) reaction force, caused by the anisotropic nature of wood. The absolute value of this lateral reaction force, expressed as lateral embedment stress, is plotted over the vertical dowel displacement in Figure 4b for the 12 mm dowel. In addition, Figure 5 illustrates the ratio between the lateral and vertical embedment stress for both dowel diameters. As obvious from Figure 4b and Figure 5, loading parallel to the principal material directions ( $0^\circ$  and  $90^\circ$ ), caused only negligible lateral reaction forces. For load-to-grain angles different from the principal material directions, a nonlinear relation of the lateral embedment stress with the vertical dowel displacement can be seen. Most interesting is that the lateral embedment stress changes sign over the loading process, which means that the lateral reaction force changes its direction with increasing vertical dowel displacement. This characteristic can be related to the anisotropic and porous wood microstructure and was found in a similar manner in the lateral dowel displacement behavior, in the case of unconstrained lateral loading (see Subsection 3.2). The vertical dowel displacement, at which the change in sign of the lateral reaction force takes place, is lowest for load-to-grain angles deviation most from the principal material directions.

As regards the absolute value of the lateral embedment stress, the highest maximum embedment stress was found for loading under  $45^\circ$  with respect to the grain (see Figure 4b). Loading under  $30^\circ$  to the grain, resulted in comparably high lateral embedment stresses. Considerably lower values were found for load-to-grain angles of  $15^\circ$ ,  $60^\circ$  and  $75^\circ$ . However, the absolute lateral embedment stress at the first peak, at a relative displacement of 2-4 mm, was found to be similar for all loading directions deviating from the principal material directions.

Expressing the lateral embedment stress relative to the vertical embedment stress, showed a similar picture, however the highest relative stress was found for loading under  $30^\circ$  to the grain, for both dowel diameters. At a vertical dowel displacement of twice the dowel diameter, the lateral reaction force amounted to about 40 % of the vertical reaction force. Loading under  $45^\circ$  to the grain showed a similar trend. For the other load-to-grain angles, the maximum lateral embedment stress was less than 20 % of the vertical embedment stress. However, at a comparable small vertical dowel displacement of less than 5 mm, the lateral embedment stress already amounted to 10-20 % of the vertical embedment stress for all loading directions deviating from the principal material directions.

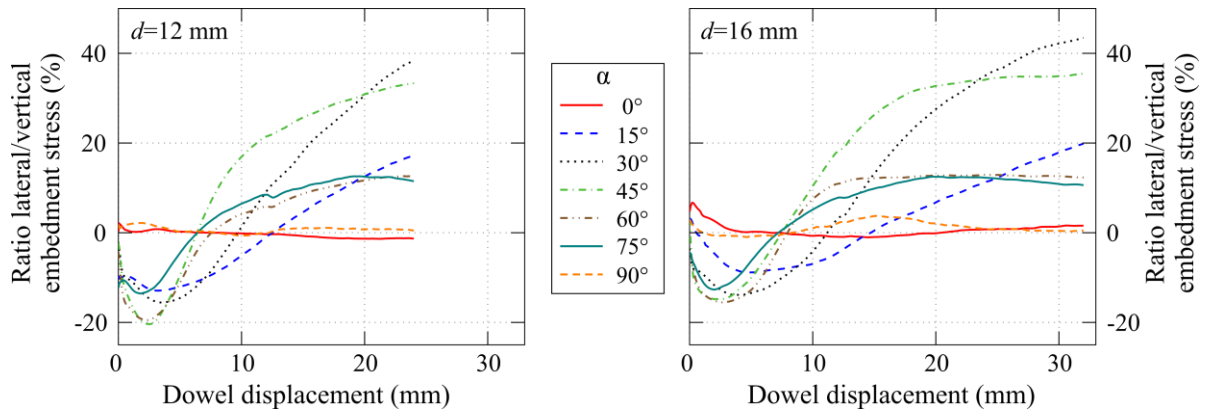


**Figure 5:** Ratio between lateral ( $f_{h,lat}$ ) and vertical embedment stress ( $f_{h,ver}$ ) gained from embedment tests under constrained lateral dowel displacement boundary conditions for  $d=12$  mm (left) and  $d=16$  mm (right).

Unloading stiffness  $K^{unload}$  and embedment strength parameters  $f_h$  plotted over the load-to-grain angle  $\alpha$  are illustrated in Figure 6. Both, embedment stiffness and embedment strength, showed a distinct dependence on the load-to-grain angle. For the definition of the presented parameters, the reader is referred to Schweigler et al (2016).

As regards the unloading stiffness  $K^{unload}$ , which represents the elastic, recoverable deformations of the structural system, a decrease in stiffness with increase in  $\alpha$  was observed for both dowel diameters. Similar results of the unloading stiffness in the quasi-elastic and elasto-plastic region were found. Considerable higher values were observed for 16 mm than for 12 mm dowels, for all load-to-grain angles. These differences, might be explained by unpreventable elastic deformations of the steel dowel in bending, which would be higher for 12 mm than 16 mm dowels. Thus, combination of the compliant embedment behavior and the compliance of the steel dowel itself leads to a fictitious softer response of the 12 mm dowel compared to the 16 mm dowel.

Different embedment strength properties are exemplarily shown for  $d=12$  mm in Figure 6 (right). In addition, these experimentally determined parameters are compared to the embedment strength calculated according to Eurocode 5,  $f_{h,EC5}$ , based on mean values of the LVL density. The embedment strength determined as the maximum embedment stress for a dowel displacement up to 5 mm,  $f_{h,5mm}$ , and the embedment strength calculated as the 2 % offset limit,  $f_{h,0.02d}$ , follow the S-shaped trend of the embedment strength with respect to the load-to-grain angle proposed by Eurocode 5. The embedment strength,  $f_{h,0.02d}$ , was found to represent best the quasi elastic limit. Compared to  $f_{h,EC5}$ , consistently lower embedment stresses were found for  $f_{h,0.02d}$ . An almost perfect match between the calculated  $f_{h,EC5}$ , and the experimentally determined  $f_{h,5mm}$  for all load-to-grain angles became obvious from Figure 6 (right). As regards the embedment strength determined at a dowel displacement of two times the dowel diameter,  $f_{h,2d}$ , considerable higher values for load-to-grain angles of  $30^\circ$  and higher, compared to the embedment strength calculated according to Eurocode 5 were found. This can be explained by the aforementioned hardening effects for large load-to-grain angles and dowel displacements, in combination of strengthening effects caused by the constrained loading situation.

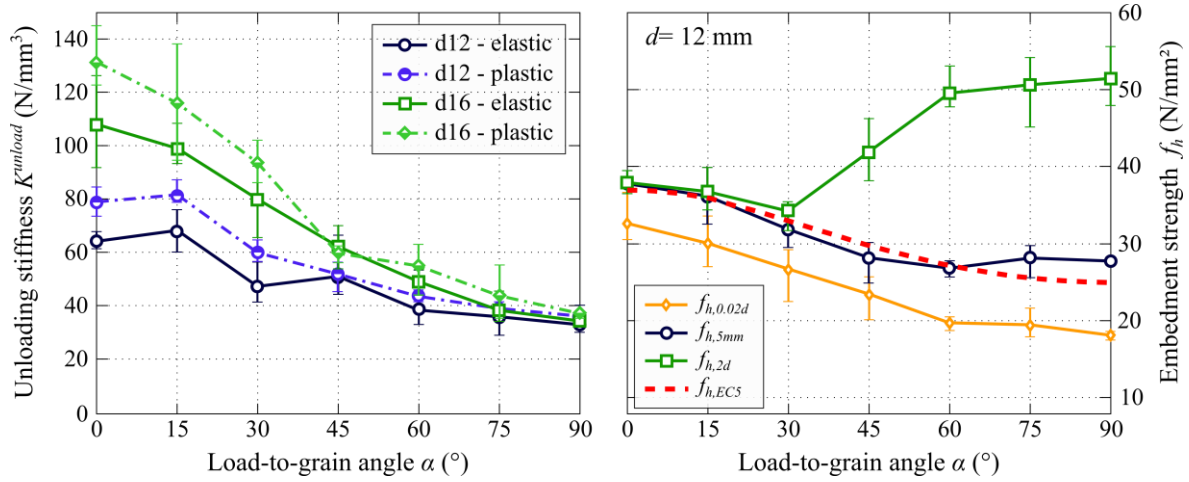


**Figure 6:** Unloading stiffness in the quasi-elastic part and elasto-plastic part vs. load-to-grain angle for the 12 mm and 16 mm dowel (left). Embedment strength properties vs. load-to-grain angle for  $d=12$  mm, including comparison to Eurocode 5-based calculation of the embedment strength (right).

### 3.2 Embedment tests under unconstrained lateral displacement boundary conditions

Results presented in the following are a summary of the findings from embedment tests under unconstrained lateral displacement boundary conditions, see Schweigler et al. (2016). A pronounced ductile embedment behavior was observed, without premature global failure of the test specimen. Thus, meaningful results up to large dowel displacements of at least equal to twice the dowel diameters could be established.

In contrast to loading with constrained lateral boundary conditions (Subsection 3.1), loading under unconstrained lateral boundary conditions by means of a pendulum, yielded pronounced lateral dowel displacements transverse to the initial vertical loading direction (see Figure 7) for load-to-grain angles that deviated from the principal material directions. Both dowel diameters, i.e., 12 mm and 16 mm, exhibited a similar behavior and therefore only general statements for both dowel diameters are given in the following. As obvious from Figure 7, loading parallel to the principal material directions, i.e., parallel to the grain (0°) and perpendicular to the grain (90°), was characterized by an almost symmetric response in terms of the displacement behavior. For loading directions deviating from the principal material directions, a nonlinear displacement path of the steel dowel was observed, which can be described as follows: The dowel first moved towards the initially softer material direction, i.e., perpendicular to the grain. Increasing the load led to a change in the displacement direction towards grain parallel loading. This behavior could be explained by the principle of minimum energy in a closed system, and consequently, the dowel displacement vector facing the direction of lowest stiffness. The change in displacement direction is expected to be a result of changing stiffness conditions due to densification of the porous cellular wood material perpendicular to the grain, which increases with increasing load.

The slip behavior, i.e., the embedment stress plotted over the dowel displacement, in dependence of the load-to-grain angle is discussed next. Figure 8a shows a three-dimensional illustration of the slip curves plotted over the load-to-grain angle, for dowels with 12 mm in diameter. Linear interpolation has been used for the areas between the experimentally determined slip curves. In Figure 8b, the corresponding slip curves are plotted separately for each load-to-grain angle. In general, a similar load-displacement behavior has been found for both dowel diameters of 12 mm and 16 mm. However, differences in the magnitude of the nominal embedment stress, dependent on the load-to-grain angle and dowel displacement, between these two dowels were observed. For discussion on this topic the reader is referred to Schweigler et al (2016).

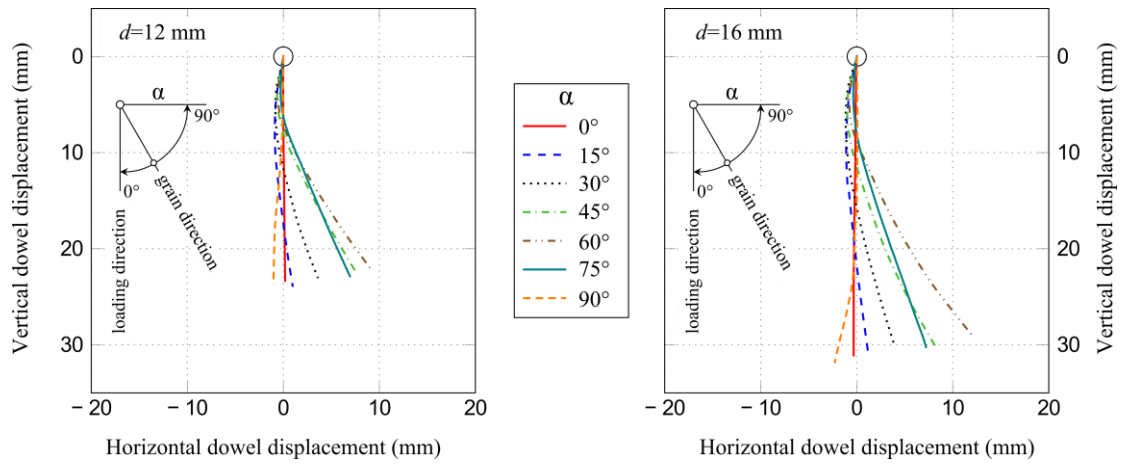


**Figure 7:** Displacement path of the vertically loaded dowel under unconstrained lateral dowel displacement boundary conditions for  $d=12$  mm (left) and  $d=16$  mm (right).

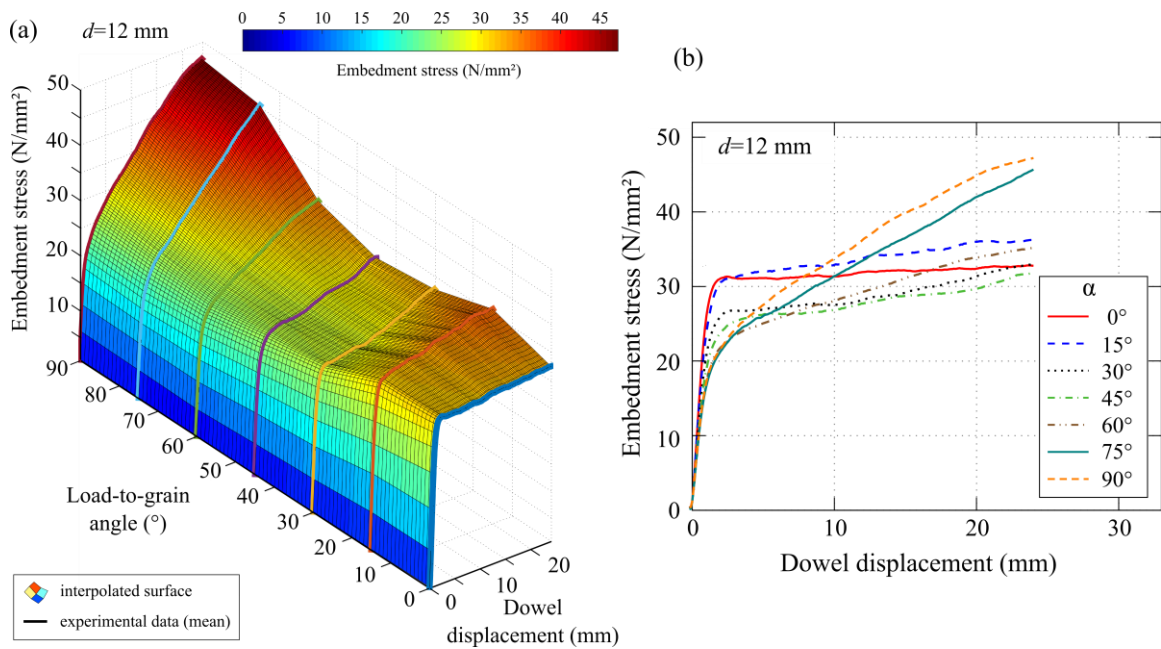


**Figure 8:** Embedment behavior under unconstrained lateral dowel displacement boundary conditions for  $d=12$  mm, (a) embedment stress plotted over the load-to-grain angle and the dowel displacement, (b) embedment stress plotted over the dowel displacement for different load-to-grain angles, Schweigler et al. (2016).

The slip curves can be simplified by a quasi-linear elastic behavior, followed by a pronounced, almost linear plastic behavior for all investigated load-to-grain angles. For loading parallel to the grain ( $0^\circ$ ) and under  $15^\circ$  to the grain, the load-displacement behavior can be characterized by an almost linear-elastic, ideal plastic response. A comparable level of the embedment stress was found for both load-to-grain angles. The slip behavior for increased  $\alpha$  between  $15^\circ$  and  $45^\circ$  was characterized by a decrease of the quasi-elastic stiffness and embedment strength, and slightly increased elasto-plastic loading stiffness with increasing load-to-grain angle (see Figure 8). For loading under  $60^\circ$  to the grain and higher, a pronounced hardening behavior for large dowel displacements became obvious. The corresponding increase of the elasto-plastic loading stiffness with increasing  $\alpha$ , could be explained by densification of the wood in the contact area below the dowel as well as by the so-called rope effect in the wood fibers. The latter effect is related to stresses parallel to the grain, which can arise for load components perpendicular to the grain, as consequence of deflection forces gained from wood fibers in bending.

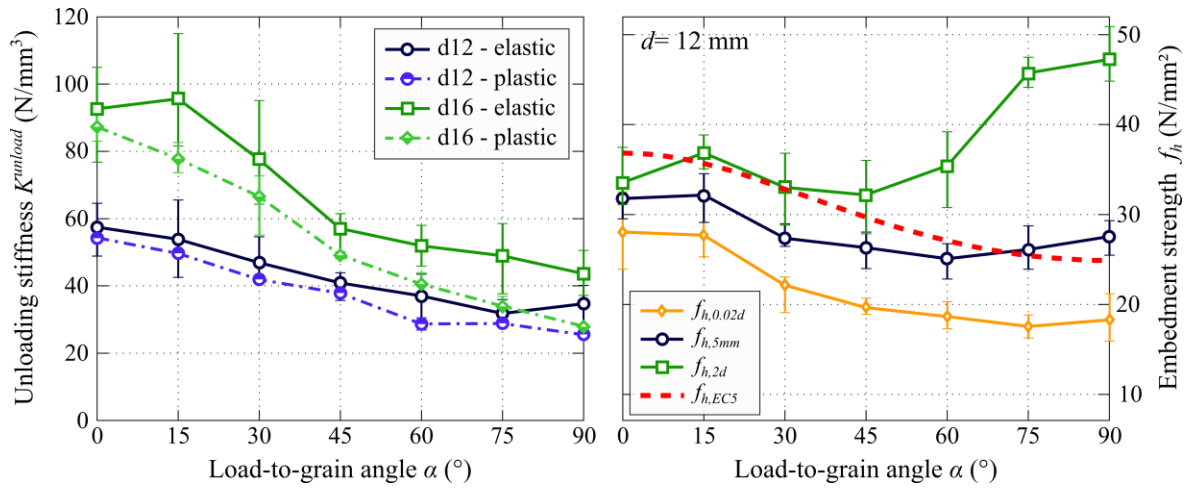


**Figure 9:** Unloading stiffness in the quasi-elastic part and elasto-plastic part vs. load-to-grain angle for the 12 mm and 16 mm dowel (left). Embedment strength properties vs. load-to-grain angle for  $d=12$  mm, including comparison to Eurocode 5 based calculation of the embedment strength (right), Schweigler et al. (2016).

Embedment properties, i.e. stiffness and strength parameters, exhibit a pronounced dependence on the load-to-grain angle,  $\alpha$ . In Figure 9, the unloading stiffness  $K^{unload}$  (left) and the embedment strength  $f_h$  (right) is plotted over the load-to-grain angle  $\alpha$ . For the definition of these parameters, the reader is referred to Schweigler et al (2016).

As regards the unloading stiffness  $K^{unload}$ , which represents the elastic recoverable deformations of the structural system, a decrease in stiffness with increase in  $\alpha$  was observed for both dowel diameters. Similar results of the unloading stiffness in the quasi-elastic and elasto-plastic region were found. Considerably higher values were observed for 16 mm than 12 mm dowels, for all load-to-grain angles.

Different embedment strength properties are exemplarily shown for  $d=12$  mm in Figure 9 (right). In addition, these experimentally determined parameters are compared to the embedment strength calculated according to Eurocode 5 based on the mean LVL density. The embedment strength determined as the maximum embedment stress for a dowel displacement up to 5 mm,  $f_{h,5mm}$ , and the embedment strength calculated as the 2 % offset limit,  $f_{h,0.02d}$ , follow the S-shaped trend of the embedment strength with respect to the load-to-grain angle proposed by Eurocode 5. As obvious from Figure 9 (right), Eurocode 5 calculations are higher than the experimental embedment strength  $f_{h,5mm}$  for small load-to-grain angles  $\alpha$ , while for large load-to-grain angles a good agreement with Eurocode 5 was seen. As regards the embedment strength determined at a dowel displacement of two times the dowel diameter,  $f_{h,2d}$ , considerable higher values for load-to-grain angles of  $60^\circ$  and higher, compared to the embedment strength calculated according to Eurocode 5 were found. This can be explained by the aforementioned hardening effects for large load-to-grain angles and dowel displacements.

### 3.3 Comparison between constrained and unconstrained embedment behavior

A comparison for a dowel diameter of 12 mm and a load-to-grain angle  $\alpha$  equal to  $45^\circ$ , between the embedment behavior under constrained and unconstrained lateral displacement boundary conditions, is exemplarily given in Figure 10. The displacement paths of the initial vertically loaded dowels are illustrated in Figure 10a, while the slip curves, expressed as embedment stresses plotted over the dowel displacement, are visualized in Figure 10b.

As regards the displacement behavior, considerable lateral dowel displacements up to about 8 mm for the 12 mm dowel loaded under  $45^\circ$  to the grain were found for loading at unconstrained lateral displacement conditions. A lateral dowel displacement with a change in the sign, as described in more detail in Subsection 3.2 became obvious. On the contrary, lateral dowel displacements at constrained dowel displacement boundary conditions were close to zero. However, small lateral

displacements, less than 1 mm, were measured. This can be explained by the fact of measuring the dowel displacement relative to the specimen surface. Lateral displacements between the horizontally quasi-fixed dowel and the deformable LVL-specimen, were caused by the evoked lateral reaction forces; even if the horizontal support device did not exhibit any lateral displacement. Therefore, strictly speaking, the dowel was not fully constrained in lateral direction, because of the compliance in the LVL specimen.

Figure 10b shows slip curves for the vertical and lateral embedment stress under constrained and unconstrained dowel displacement boundary conditions. In general, a similar load-displacement behavior for both loading conditions was found, i.e., a quasi-linear elastic behavior followed by an almost linear elasto-plastic behavior with considerable hardening at large dowel displacements. Constrained loading exhibited, as compared to unconstrained loading, a slightly higher quasi-elastic loading stiffness and a significantly higher elasto-plastic loading stiffness. The embedment stress at a dowel displacement of twice the dowel diameter, i.e., 24 mm, was found to be 41.9 N/mm<sup>2</sup>, which is about 30% higher than for unconstrained conditions. Prescribing a vertical dowel displacement at constrained lateral boundary conditions evoked a lateral reaction force, which is in the following expressed as nominal embedment stresses. Qualitatively the sign of the lateral embedment stresses correlated well with the sign of the lateral dowel displacement from unconstrained displacement boundary conditions and showed a similar trend. The mean value of the lateral embedment stress at the maximum displacement limit amounted to 13.9 N/mm<sup>2</sup>. Thus, prescribing a vertical dowel displacement at constrained lateral boundary conditions evoked lateral embedment stresses of more than 30% of the vertical stress. Considerable lateral embedment stresses were also found for small vertical dowel displacements. The lateral embedment stress at a dowel displacement of 2.5 mm amounted to 5.8 N/mm<sup>2</sup>, which was about 20% of the corresponding vertical embedment stress. This is particularly interesting, since EN 383 (2007) prescribes embedment testing up to 5 mm dowel displacement which means that even in this displacement region, pronounced lateral reaction forces will be encountered in case of constrained loading conditions. This should consequently be mentioned and discussed in the test standard.

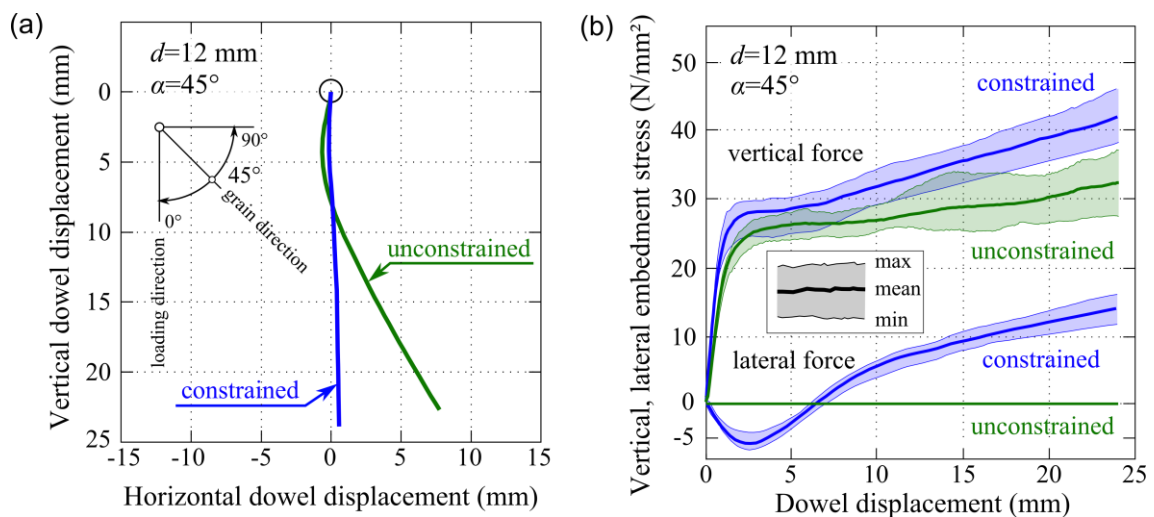


**Figure 10:** Comparison of the embedment behavior under constrained and unconstrained lateral dowel displacement boundary conditions for  $d=12$  mm at  $\alpha=45^\circ$ . (a) dowel displacement paths of the vertically loaded dowels, (b) vertical and lateral reaction forces expressed as embedment stresses.

As regards the unloading stiffness, a similar trend for both loading situations was observed. Constrained as well as unconstrained loading yielded in a decrease of the embedment unloading stiffness with increasing load-to-grain angle for both dowel diameters, as well as for both unloading in the quasi-elastic and elasto-plastic displacement state. Also the differences between the unloading stiffness of the two dowel diameters were consistent for both test series. Interestingly, constraining the dowel displacement resulted in consistently higher unloading stiffness parameters than for unconstrained conditions. This might be explained by stiffening effects caused by constrained load

application. This theory might be supported by the fact of a slightly larger unloading stiffness in the elasto-plastic range compared to the quasi-elastic range, since a more pronounced stiffening can be expected for larger dowel displacements. In contrast, exactly the opposite, i.e. slightly larger unloading stiffness in the quasi-elastic part, became obvious for unconstrained loading, where no stiffening effects can be expected.

Similar trends were also observed for the loading stiffness in unconstrained testing, which are not discussed in detail in this report. However, for testing under constrained lateral displacement situations, trends were not as clear. The reason for this is expected to lie in displacement measurement setup, namely in the use of only one pair of cameras on one side of the test specimens. Pronounced asymmetric displacements, particularly during the first loading path became obvious in the analysis of the test series with unconstrained dowel displacement boundary conditions, where two pairs of cameras for displacement measurements have been used.

An impact of the lateral displacement boundary condition on the embedment strength could be illustrated with the two test series. The embedment strength properties were found to be lower for unconstrained compared to constrained loading situations. In the latter case, strength at the 5 mm displacement limit was found to be very close to the Eurocode 5 values. The most pronounced differences between both test series were found for the load-to-grain angles of  $45^\circ$  and  $60^\circ$ , particularly in their plastic behavior. Constraining the dowel displacement yields a remarkable increase of the hardening effect for these load-to-grain angles. The vertical embedment strength of the other load-to-grain angles were comparable with the one from unconstrained loading conditions. However, already small deviations in the loading direction from the principal material directions ( $0^\circ$  and  $90^\circ$ ), i.e. loading at  $15^\circ$  and  $75^\circ$  to the grain, caused considerable lateral embedment stresses of more than 15 % of the vertical embedment stress. Loading under  $30^\circ$  and  $45^\circ$  to the grain yields even lateral forces up to 40 % of the vertical forces. Thus, these lateral forces under constrained loading conditions additionally introduce considerable forces to the surrounding timber matrix, which have to be considered in the design of such connections.

#### **4 Conclusion, outlook and future collaboration with the host institution**

The main objective of the herein presented STSM at the *Linnæus University* (Växjö, Sweden) was to carry out experimental investigations of the embedment behavior of screw-reinforced LVL under constrained lateral displacement conditions. Full-hole embedment test at seven different loading directions with respect to the grain for two different dowel diameters up to dowel displacements of two times the dowel diameter were conducted. A biaxial test setup allowed to record, in addition to the vertically applied displacement loading, also the lateral reaction force, evoked by the anisotropic material behavior under constrained lateral displacement conditions. In addition, the embedment behavior of LVL under unconstrained lateral displacement conditions was experimentally determined prior to the STSM at the authors home institute. Results from these two test series, representing the two limit cases of the embedment behavior, were used for comparison purposes, in order to investigate the influence of the displacement boundary condition on the embedment behavior.

The main outcome of the two test series can be summarized as follows:

- Pronounced ductile embedment behavior up to dowel displacements of twice the dowel diameter.
- Nonlinear load-displacement behavior, with a decrease in quasi-elastic embedment strength and stiffness, and increase of elasto-plastic embedment strength and stiffness for increasing loading direction with respect to the grain direction.

Constrained loading gave in comparison to unconstrained loading:

- An additional lateral embedment stress up to 40 % of the vertical embedment stress.
- Higher embedment stresses for the load-to-grain directions between parallel and perpendicular to the grain.

- Stronger hardening effect in the plastic state, especially for loading under 45° and 60° to the grain.
- Stiffer elastic response, expressed by the unloading stiffness.

The comprehensive dataset of the embedment behavior under constrained and unconstrained displacement boundary conditions is intended to be used for parameterized definitions of the embedment stresses. During this STSM, parameterization methods have been discussed, described in this report and will be further refined and optimized for application on the results from both test series. Especially on this topic, and on the interpretation of the strain distributions, gained from DIC measurements, an ongoing discussion and collaboration with the host institute is envisaged. A parameterized description of the embedment behavior is expected to facilitate the comparison with previous data and include a proposal for design equations in future standards. The output of these tests is also expected to enhance the understanding of wood embedment properties in general and to support discussions related to testing regulations provided in testing standards.

## 5 Foreseen publications resulting from the STSM

The findings from the experimental investigations on the embedment behavior under constrained lateral displacement boundary conditions, as well as the study on parameterization strategies for steel dowels embedded in timber are foreseen to be published in a joint peer-reviewed journal paper of the *Linnæus University* and the *Vienna University of Technology*.

## Acknowledgements

I would like to thank the steering committee of the COST Action FP 1402 for providing funding for this experimental campaign and giving me the chance of working together with colleagues at the Linnæus University. In particular, Thomas Bader, Michael Dorn and Bertil Enquist are thanked for their support during the experimental program and for the fruitful discussions on the results gained from this STSM. In addition, Johan Vessby is gratefully acknowledged for providing me access to the laboratory and facilities of the Department of Building Technology at Linnæus University.

## References

- Bader, T.K., Schweigler, M., Hochreiner, G., Enquist, B., Dorn, M., Serrano, E.: *Experimental characterization of the global and local behavior of multi-dowel LVL-connections under complex loading*. Mater Struct, pp.1–18, 2015a.
- Bader, T.K., Schweigler, M., Hochreiner, G., Serrano, E., Enquist, B., Dorn, M.: *Dowel deformations in multi-dowel LVL-connections under moment loading*. Wood Mat Sci Eng 10(3), 216–231, 2015b.
- Bader, T.K., Schweigler, M., Serrano, E., Dorn, M., Enquist, B., Hochreiner, G.: *Integrative experimental characterization and engineering modeling of single-dowel connections in LVL*. Constr Build Mater 107, 235–246, 2016.
- Bleron, L., Duchanois, G.: *Angle to the grain embedding strength concerning dowel type fasteners*. Forest Prod J 56(3), 44–50, 2006.
- Ehlbeck J, Werner H.: *Softwood and hardwood embedding strength for dowel-type fasteners*. In: CIB-W18 Meeting 25, Paper 25-7-2. Aarhus, Denmark, 1992.
- EN 383: Timber structures - Test method - *Determination of embedment strength and foundation values for dowel type fasteners*. European Committee for Standardization (CEN), 2007.
- Foschi, R.: *Load-slip characteristics of nails*. Wood Sci 7(1), 69–76, 1974.

---

Franke, S., Quenneville, P.: *Embedding behavior of LVL and radiata pine lumber*. In: Proceedings of 11<sup>th</sup> World Conference on Timber Engineering, Italy, 2010.

Hankinson, R.L.: *Investigation of crushing strength of spruce at various angles of grain*. Air Force Information Circular 3(259), 1921.

Hochreiner, G., Bader, T., de Borst, K., Eberhardsteiner, J.: *Stiftförmige Verbindungsmittel im EC5 und baustatische Modellbildung mittels kommerzieller Statiksoftware* (in German). Bauingenieur 88, 275–289, 2013.

Hübner, U., Bogensberger, T., Schickhofer, G.: *Embedding strength of European hardwoods*. Proceedings of CIB-W18, Paper pp. 41–7, 2008.

Johansen, K.: *Theory of timber connections*. In: International Association of Bridge and Structural Engineering, vol. 9, pp. 249–262, 1949.

Sandhaas, C., Ravenshorst, G., Blass, H., van de Kuilen, J.: *Embedment tests parallel-to-grain and ductility aspects using various wood species*. Eur J Wood Wood Prod 71(5), 599–608, 2013.

Sawata, K., Yasumura, M.: *Determination of embedding strength of wood for dowel-type fasteners*. J Wood Science 48(2), 138–146, 2002.

Schweigler, M., Bader, T.K., Hochreiner, G., Unger, G., Eberhardsteiner, J.: *Load-to-grain angle dependence of the embedment behavior of dowel-type fasteners in laminated veneer lumber*, accepted for publication in Constr Build Mater, 2016.

## **Appendix**

Confirmation by the host institute (Building technology, Linnæus University) of the successful execution of the STSM.



## To the Core Group of the COST Action FP1402

### **Host approval of completed STSM within the framework of COST FP1402**

**Topic title: “Experimental characterization and parameterization of the load-to-grain angle dependent embedment behavior of dowel-type fasteners in laminated veneer lumber (LVL)”.**

I hereby confirm that Michael Schweigler (PhD student at the Institute for Mechanics of Materials and Structures, Vienna University of Technology) has successfully performed the Short Term Scientific Mission at the Department of Building Technology, Linnaeus University in Växjö during the period 9-27 May, 2016.

The STSM was predominantly dedicated to carrying through mechanical tests in the laboratory of the department but also included a discussion on evaluation and parameterization strategies. More specifically, Michael Schweigler performed during his visit to the university embedment tests in a biaxial test setup, where reaction forces caused by prescribed displacement paths could be quantified. This is particularly important for displacement paths deviating from the main axis of the anisotropic wood material. A first evaluation of selected tests indicates the relevance of this effect, already up to displacement limits currently specified in testing standards.

Michael Schweigler’s report has covered all the details, which we have discussed during the STSM, in addition to presenting experiments and selected results, which he partly carried out at the Vienna University of Technology after his visit to Växjö. Further evaluation work will be performed in order to exploit the potential of full-field deformation measurements in terms of gaining insight into load-transfer mechanisms. It is intended that results of this work will lead to a joint scientific publication.

Michael Schweigler’s experiments not only contribute to an experimental database but also highlight opportunities of how to account for complex material behavior in design rules in standards. We are truly grateful for the opportunity provided by COST FP1402 for this STSM.

Sincerely yours,

Johan Vessby, Building technology, Linnaeus University